Title

The cold-inducible RNA-binding protein RBM3 stabilises viral mRNA at the cooler temperatures of the upper respiratory tract.

Authors

Hannah L Coutts[1], Hannah L Turkington[1], Stefano Bonazza[1], Erin M P E Getty[1], Swathi Sukumar[1], Ultan F Power[1], David G Courtney[1]

Affiliations

1 Wellcome-Wolfson Institute for Experimental Medicine, Queen's University Belfast, Belfast BT9 7BL, UK

Abstract

Temperature regulation is a key aspect of homeostasis, and several systems are involved in orchestrating adjustments in gene expression at the cellular level. One such factor is RBM3, a cold-inducible RNA-binding protein implicated in several aspects of mRNA processing and regulation. The upper respiratory tract serves as a unique environment regarding temperature regulation. Physiologically, the lower tract is relatively stable at 37°C, while the upper tract fluctuates at or below 33°C. Adapting to this temperature differential, and the subsequent differences in transcriptome and proteome, is essential for respiratory viruses that infect and cause disease in the lower tract while simultaneously replicating and transmitting from the upper tract. At present, our understanding of the molecular mechanisms underlying influenza virus infection at cooler temperatures is lacking. Unsurprisingly, RBM3 protein levels are highest in nasopharyngeal tissue. Coupled with its known role in positively regulating bound RNA, it is an appealing candidate for manipulation by respiratory viruses. We found siRNA knockdown of RBM3 significantly decreased viral replication. To disentangle the direct effect of RMB3 from the shift in global gene expression at colder temperatures, we generated an A549 cell line constitutively overexpressing RBM3 at 37°C. Overexpression resulted in a significant increase in levels of viral replication. RBM3 was found to readily bind viral NP mRNA during infection and prolong the half-life of these transcripts. In contrast, an RBM3 RNA binding null mutant reverses this phenotype, validating that direct interaction of RBM3 has a stabilising effect on viral transcripts. The proviral nature of increased RBM3 levels was further validated in the more clinically relevant model of well-differentiated primary nasal epithelial cells. These data suggest a role for RBM3 in supporting influenza virus replication in the nasopharyngeal tract. Understanding IAV replication in this

environment could prove fundamental to elucidating the mechanisms of influenza transmission and reassortment.

Author Summary

To establish a productive infection, respiratory viruses must overcome or adapt to several systems within the body. One such obstacle is the temperature gradient of the respiratory tract. The upper respiratory tract, which serves as the primary route of viral transmission, provides the virus with a drastically different cellular environment compared to the lower respiratory tract, due to differences in growth temperatures. Here, we detail our investigation into the differences in the RNA binding protein (RBP) landscape between 33°C and 37°C. Our aim was to identify specific RBPs that are upregulated at 33°C and to explore their role in the influenza A virus (IAV) lifecycle, thereby advancing our knowledge of the molecular mechanisms underlying IAV infection in the upper respiratory tract. Through a combination of molecular virology and mass spectrometry, we identified a cold-inducible RBP, RBM3, as an important post-transcriptional regulator of IAV nucleoprotein (NP) mRNA. We show that RBM3 binds specifically to viral NP mRNA, stabilising the mRNA, and ultimately promoting the production of infectious virions, while abolishing the RNA binding capabilities of RBM3 reversed this effect. Overall, we find that enhanced RBM3, as seen in the upper respiratory tract, positively influences viral replication.

57 ## Introduction

58 Respiratory viruses are an ever-present pandemic concern, due in part to their airborne mode
59 of transmission (1). While severe pathology from respiratory viruses such as influenza A virus
60 (IAV) or SARS-CoV-2 generally occurs due to viral replication in the lower respiratory tract
61 (LRT), viral transmission predominantly occurs from small droplets and aerosols from the
62 upper respiratory tract (URT) (1–4).Thus, advancing research into the unique cellular
63 environment of the nasopharyngeal epithelium is crucial to furthering our understanding of
64 viral transmission (5) and will ultimately aid public health bodies in developing the next
65 generation of nasal vaccines to boost mucosal immunity (6,7). A key aspect of this
66 environment is the lower physiological temperature at which nasopharyngeal epithelial cells
67 grow, generally at or below 33°C, compared to the average core body temperature around
68 37°C (8). This seemingly small difference in temperature can have wide-ranging effects on
69 normal cell biology, and by extension viral replication kinetics (9).

70 Molecular interactions and reaction kinetics are governed by thermodynamics, and
71 temperature constitutes a fundamental factor in regulating such processes. Consequently,
72 the interaction landscape, concerning both nucleic acids and proteins, is considerably
73 different in colder environments (10). Such variations can result in the misfolding of proteins
74 or RNA, dramatically affecting the cell as a whole (10–12). Meanwhile, differences in affinities
75 between RNA-binding proteins (RBPs) and target RNAs can have substantial effects on an
76 array of post-transcriptional processes (13). Although differences in transcript and protein
77 production have been observed with changing temperatures (14,15), it is not well understood
78 how, on a global level, growth temperature affects the RBPs that bind to cellular mRNAs.

79 The central aim of this study was to better understand the cellular landscape encountered by
80 respiratory viruses, with a focus on IAV, and to determine how altered growth temperature
81 affects post-transcriptional regulation of viral mRNAs. Specifically, this work investigated how
82 the overall landscape of RBPs bound to mRNAs, termed the RBPome, of lung epithelial cells
83 (A549 cells) differs between growth temperatures of 37°C and 33°C. Previous studies have
84 recently demonstrated how important the host RBPome is to viral replication, affecting
85 critical aspects of viral RNA regulation (16,17), such as nuclear export (18), translational
86 control (17) and replication (19).

87 The data presented here describes a large variation in RBPs associating with cellular mRNAs,
88 finding a comparable number of RBPs whose association with mRNA is enriched or depleted
89 at 33°C when compared to that of 37°C. One of the most interesting RBPs highlighted by this
90 study, significantly enriched in the 33C dataset, was RNA Binding Motif 3 (RBM3). This RBP is
91 a classic cold-inducible protein and is reported to be important for the management of
92 cellular stress under hypothermic conditions (20,21). Moreover, it was recently identified by
93 ourselves and colleagues in an IAV mRNA interactome screen (22). Here, we uncovered that
94 RBM3, through its stabilisation of viral transcripts, is wholly pro-viral during IAV infection of
95 A549 cells. Importantly, this pro-viral role was further validated in well differentiated primary
96 nasal epithelial cells (PNAECs) from multiple donors through antisense oligonucleotide (ASO)-
97 mediated overexpression of RBM3 followed by infection.

98 Overall, these findings demonstrate a vastly different regulatory landscape for RNA likely
99 exists in the human URT, where cellular growth temperatures are just a few degrees lower
100 than core body temperature. This has an important impact on the replication of respiratory
101 viruses, providing a contrasting environment to that of the lower respiratory tract, which
102 viruses must adapt to and overcome in order to transmit efficiently.

103 **Results**

104 The cold RBPome of A549 cells reveals RBM3 as a significantly enriched mRNA interactor

105 As previously mentioned, the temperature gradient normally observed in the respiratory tract
106 is known to yield distinct variations in cellular transcriptomes and proteomes (14,15) (Figure
107 1A). To identify specific RBPs that are differentially regulated through temperature, we
108 employed RNA Interactome Capture (RIC) (23) on A549 cells incubated for 48 h at 33°C or
109 37°C. This method allowed for the purification and identification of poly(A) RNA-binding RBPs
110 via UV crosslinking and mass spectrometry (Figure 1B). Quality control of the protein samples
111 to be analysed by MS was assayed by silver staining, highlighting the presence of distinct
112 protein compositions between experimental conditions (Figure 1C). We observed clear
113 differences in band patterns between the 33°C and 37°C in the pulldown samples indicative
114 of the differences between the two proteomes, which were evaluated by LC-MS/MS. The
115 resulting dataset was analysed for enrichment of RBPs in the 33°C compared to the 37°C
116 samples (Figure 1D). Adjusted P values were calculated with a cutoff of $p<0.05$. Between these
117 datasets, we identified a considerable number of RBPs that were preferentially enriched in
118 either temperature. Interestingly, a total of 209 RBPs were shared between 33°C and 37°C
119 (Figure 1E and 1F). Of the total 423 RBPs identified across all datasets, 296 were found to be
120 significantly regulated by alterations in growth temperature. Those that were present in both
121 datasets, but significantly enriched at 33°C, included RBM3, YBOX1, HNRNPC, RBM47 and
122 SND1 (Supplementary Table 1 and 2). Overall, these datasets are important evidence that the
123 RBP environment of the cell is very plastic. Several factors are selectively overrepresented at
124 cold temperatures and thus could play a role in respiratory virus infections.

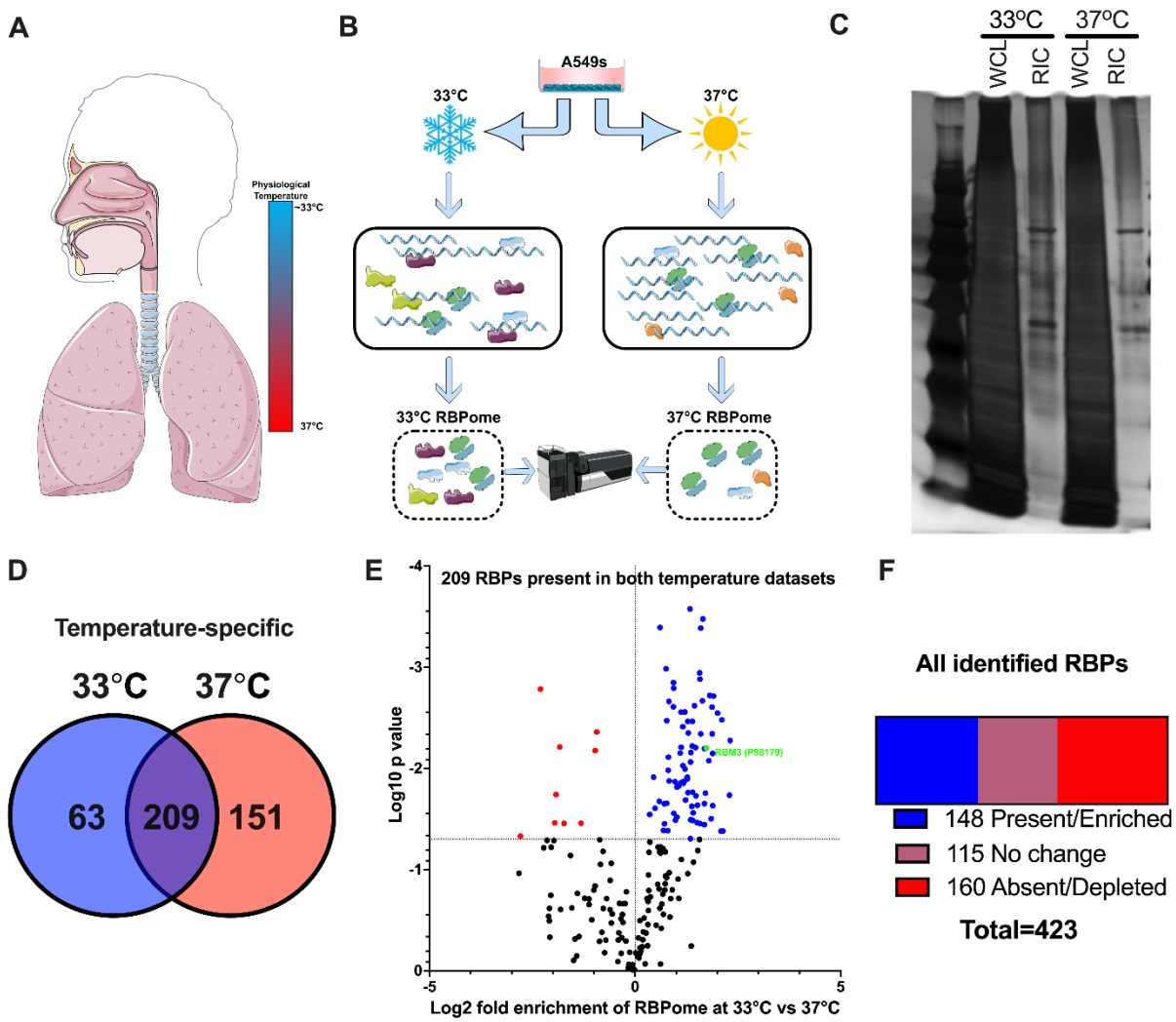

Figure 1 – Cooler growth temperatures vastly alter the RBPome of A549 cells.

***(A)** Schematic representation of the temperature gradient between the URT and LRT. **(B)** Schematic of the workflow for RIC in A549 cells incubated at 33°C or 37°C. **(C)** Representative silver stain of a gel with the RIC whole cell lysate input (WCL) and pulldown (RIC) samples from protein populations at 33°C and 37°C. **(D)** Venn diagram showing RBPs present in either 33°C datasets, 37°C datasets or both. **(E)** Volcano plot showing the enrichment of RBPs isolated from A549 33°C and 37°C pulldown samples. **(F)** Representation of the proteins significantly altered between datasets, whether by presence/absence or enrichment/depletion. Datasets derived from 3 independent biological samples.*

Loss of RBM3 negatively regulates IAV replication in A549s

One of the top hits enriched in the 33°C dataset was RBM3. This cold-inducible protein was recently identified by ourselves and our colleagues when performing an IAV A/WSN/33 NP mRNA interactome screen, and therefore presented an attractive option as an RBP that could play a role in IAV replication in the URT. Firstly, to investigate whether RBM3 impacts IAV replication we performed siRNA-mediated knockdown of RBM3 in A549 cells, followed by infection by WSN at an MOI 0.01 for 48 h. qPCR analysis confirmed effective knockdown with

140 a >95% decrease in RBM3 mRNA levels compared to a nonspecific control siRNA (NSC) (Figure
141 2A). Total RNA was harvested at 0, 8, 24 and 48 hours post infection (hpi), and levels of viral
142 mRNA were analysed via qPCR. Overall, depletion of RBM3 resulted in a significant decrease
143 in viral HA, NA, NP and M2 mRNA at 24 and 48 hpi (Figure 2B and Supp Figure 1). Most notably,
144 we observed a nearly four-fold decrease in levels of NP mRNA at 24 hpi (Figure 2B). Not
145 surprisingly, this negative impact on viral transcript levels translated through to virus
146 production, resulting in a significant drop in viral titres below the level of detection (Figure
147 2C).

148 Recently, the splicing factor Heterogenous Nuclear Ribonucleoprotein H1 (HNRNPH1), has
149 been identified to be the temperature-dependent regulator of RBM3 (13). In brief, RBM3 pre-
150 mRNA contains exon 3a, between exons 3 and 4, whose inclusion targets RBM3 mRNA for
151 decay via the nonsense-mediated decay (NMD) pathway (24). At 37°C HNRNPH1 binds only
152 weakly to exon 3a, resulting in the inclusion of the poison exon and a decrease in RBM3 levels.
153 However, at cooler temperatures (30-33°C), HNRNPH1 strongly binds within exon 3a,
154 resulting in the exclusion of the poison exon and a robust expression of RBM3 (13). Here, we
155 sought to characterise the inclusion of RBM3's poison exon in A549 cells, and to assess the
156 role of HNRNPH1 as a regulator of RBM3 during IAV infection. A549 cells were transfected for
157 48 h with either siNSC or an siRNA targeting HNRNPH1 (siH1), then treated with either DMSO
158 or cycloheximide (CHX) (40 µg/mL), for 16 h. CHX treatment was used to inhibit NMD,
159 preventing the degradation of RBM3 transcripts containing the poison exon, thereby making
160 the visualisation of the poison exon easier. Total RNA was harvested 16 h post-treatment and
161 RBM3 poly(A) cDNA was generated by reverse transcription. The cDNA was PCR amplified
162 using primers spanning RBM3 exons 3 and 4, so that transcripts including exon 3a would
163 generate longer amplicons. From Figure 2D inclusion of exon 3a is clearly visible for the

164 samples that were treated with both the siHNRNPH1 and CHX, and to a much lesser extent
165 the siHNRNPH1/DMSO-treated sample. Further quantification of exon 3a inclusion by qPCR
166 showed a nearly 11-fold increase for siHNRNPH1/CHX-treated samples compared to
167 siHNRNPH1/DMSO-treated samples (Figure 2E).

168 These data confirmed that the regulation of RBM3 in A549 cells is similar to that described
169 for induced pluripotent stem cell (iPSC)-derived neurons (13). We next investigated whether
170 knockdown of HNRNPH1 would downregulate expression of RBM3 and mirror siRBM3
171 knockdown cells. A significant decrease in RBM3 transcript levels was confirmed by qPCR
172 upon transfection with siH1 (Figure 2F). HNRNPH1-depleted A549 cells were then infected
173 with WSN (MOI 0.01), and NP mRNA transcript levels were quantified at 0, 8, 24 and 48 hpi.
174 qPCR analysis revealed a significant reduction in viral transcripts in cells transfected with siH1
175 (Figure 2G). This again translated to a significant decrease in viral titres from siH1 treated
176 cells. (Figure 2H). Taken together, abrogation of RBM3 expression, through siRNAs targeting
177 directly RBM3 or indirectly via HNRNPH1, has adverse effects on IAV replication, and may
178 affect the post-transcriptional regulation of viral mRNA.

179

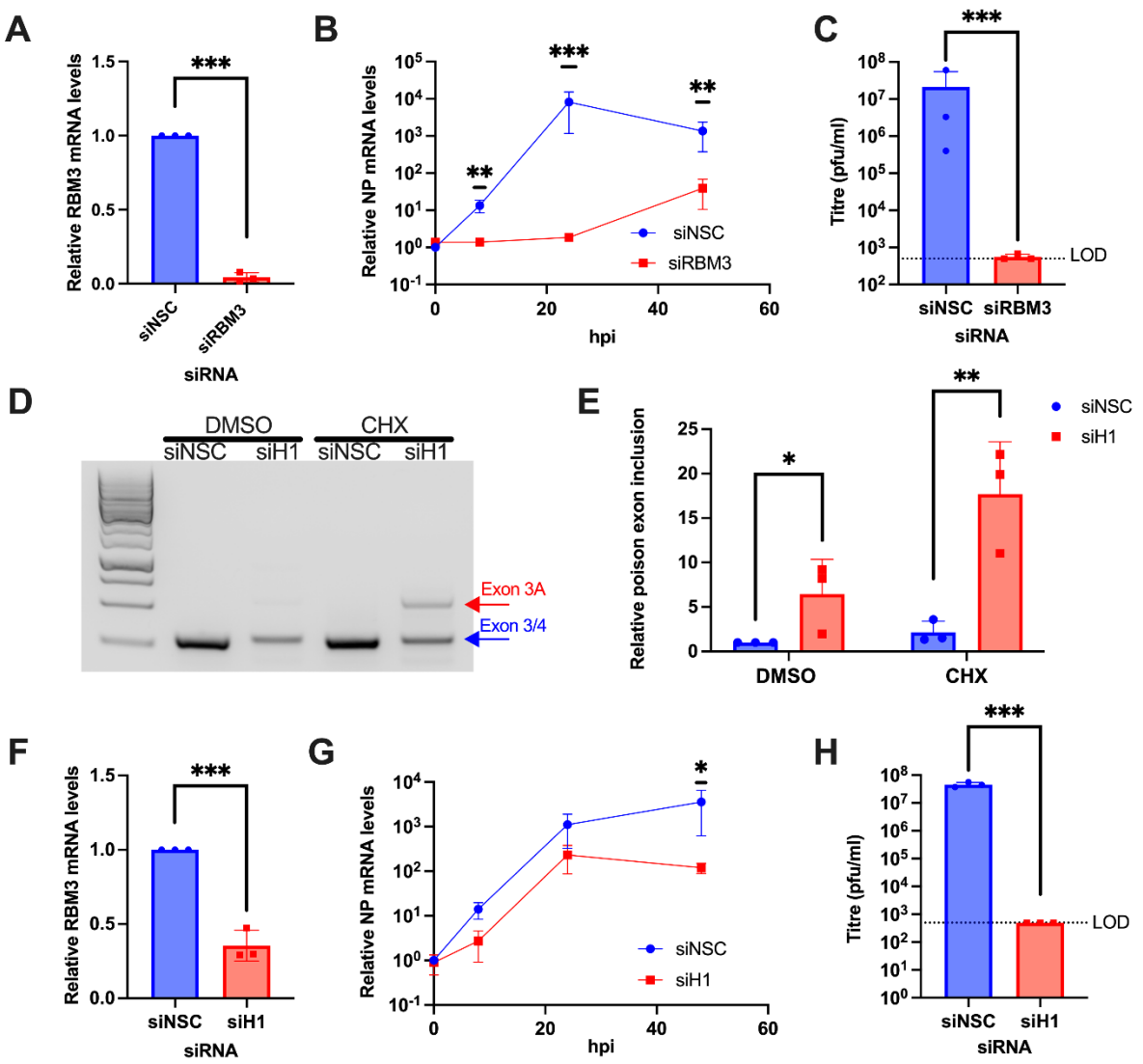

Figure 2 – Reducing RBM3 levels in A549 cells greatly inhibits IAV replication.

(A) *Quantification of RBM3 knockdown using RBM3-targeting siRNAs (siRBM3) compared to a nonspecific control siRNA (siNSC).* ***(B)*** *Transcription levels of NP mRNA in siRBM3 or siNSC treated A549 cells infected with WSN at 37°C.* ***(C)*** *Viral titres 72 hpi with WSN MOI 0.01 in siRBM3 or siNSC treated cells.* ***(D)*** *DNA gel showing inclusion of RBM3's poison exon, exon 3a. Cells were treated with siHNRNPH1 or siNSC and further treated 48 hours post-transfection with DMSO or CHX.* ***(E)*** *qPCR quantification of poison exon inclusion in the samples from Fig. 2D.* ***(F)*** *Quantification of RBM3 mRNA levels in siHNRNPH1 (siH1) A549 cells compared to siNSC treated cells.* ***(G)*** *Transcription levels of NP mRNA in siHNRNPH1 or siNSC treated A549 cells infected with WSN at 37°C. (**H**) Viral titres 72 hpi with WSN MOI 0.01 for siHNRNPH1 or siNSC treated cells.*

RBM3 overexpression increases IAV replication and binds NP mRNA

On identifying RBM3 as a potentially important RBP during IAV replication, we sought to determine whether this pro-viral phenotype arises from a direct interaction between RBM3 and viral RNA. However, as evidenced from the RIC MS, the cold environment affects the host globally, and it would be difficult to ascertain the effect of RBM3 alone on viral replication at

194 33°C. To circumvent this limitation, a cell line expressing cold-induced levels of RBM3 at 37°C
195 was needed. First, a panel of cell lines commonly used to study respiratory viruses was
196 assessed to determine their cold responsiveness, quantified by their ability to induce RBM3
197 when cultured at 33°C for 48 h. Primary nasal epithelial cells (PNECs) were used as a positive
198 control as it was expected that these would be highly responsive to cooler growth
199 temperatures. RNA was extracted and the levels of RBM3 expression were quantified by
200 qPCR, normalised to the levels observed with culturing at 37°C for each cell type (Figure 3A).
201 While PNECs were the greatest responders, with an approximate 7-fold increase in RBM3
202 mRNA levels, A549s and 293Ts both demonstrated a >3-fold increase in RBM3 levels.
203 Considering that immortalised cells can be manipulated to a greater extent that PNECs, we
204 proceeded to use A549s to develop greater mechanistic insights into the role of RBM3 during
205 IAV infection. A lentivirus-mediated stably overexpressing RBM3-Flag, clonal A549 cells line,
206 termed A549-RBM3+, was established that could be cultured at 37°C. Upon quantification by
207 qPCR, RBM3 levels were found to be >3-fold increased over an empty vector control line
208 (Figure 3B), mimicking the levels seen upon culturing of parental A549s at 33°C. Viral
209 production was then quantified in these A549-RBM3+ cells, with RBM3 overexpression
210 inducing a significant increase in viral titres of >3.5-fold (Figure 3C). Having these cell lines in
211 place, a direct interaction between RBM3 and viral transcripts could next be established.
212 Using RBPmap (25) and the published RBM3 binding motif (minimally GSNGSNG) (26), the
213 number of RBM3 high-confidence binding motifs on WSN transcripts was predicted (Figure
214 3D). While every transcript contained at least 1 putative RBM3 motif with $p<0.05$, NP mRNA
215 was predicted to have multiple highly significant binding motifs with 3 sites of $p<0.001$. These
216 data, coupled with the previously published NP mRNA interactome dataset, suggest that
217 RBM3 could directly interact with NP mRNA (22). To confirm this hypothesis CLIP-qPCR was

218 performed in which A549-RBM3+ cells were infected at MOI 3 for 6 h, then UV crosslinked,
219 and subjected to FLAG immunoprecipitation. Finally, the covalently bound RNA was released
220 by proteinase K digestion, purified and analysed by qPCR. Flag-tagged RBM3 was efficiently
221 pulled down by an anti-Flag immunoprecipitation (Figure 3E), with Actin used as a control to
222 show that this enrichment was specific. Finally, RBM3-bound RNA was quantified by qPCR.
223 We evaluated whether NP mRNA was bound to RBM3, based on the presence of multiple
224 predicted high confidence motifs. We also quantified levels of HA mRNA as a likely non-
225 interactor and Actin mRNA as a host mRNA. We observed a strong and significant enrichment
226 of NP mRNA between the RBM3 and no primary antibody control samples, while no
227 enrichment in HA or Actin levels were observed, indicating little or no binding was by RBM3.
228 Taken together, these data indicate that an increase in RBM3 expression positively regulates
229 viral replication kinetics and establish a direct interaction between RBM3 and NP viral mRNA
230 transcripts.

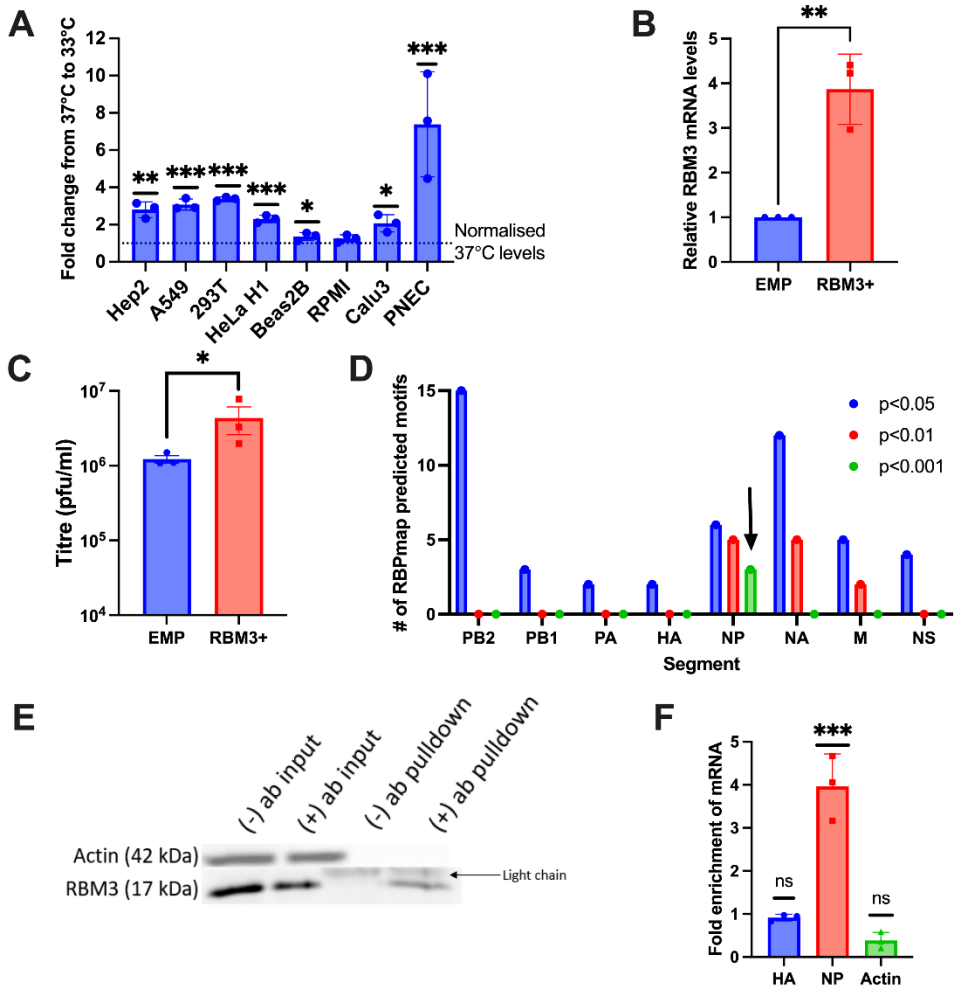

Figure 3 – RBM3 directly associates with viral transcripts, increasing overall viral replication.

(A) *Cold-responsiveness of a panel of cell lines and primary nasal epithelial cells (PNECs) as determined by the induction of RBM3 expression by qPCR over 48 h and normalised to 37°C levels.* ***(B)*** *Generation of a lentiviral RBM3 overexpression (RBM3+) A549 cell line alongside a control empty vector line (EMP).* ***(C)*** *Titres of WSN at 72 hpi after an MOI 0.01 infection in EMP or RBM3+ A549 cells.* ***(D)*** *RBPmap predicted RBM3 binding motifs for each WSN positive strand segment, separated by predicted confidence of each motif.* ***(E)*** *Western blot showing input and pulldown samples for CLIP-qPCR, blotting for Actin and overexpressed RBM3-Flag.* ***(F)*** *qPCR quantification of the RNA extracted from CLIP samples demonstrated a significant increase in viral NP mRNA levels with minimal differences in HA or Actin transcripts, when comparing RBM3 to no antibody control pulldowns.*

Overexpression of RBM3 selectively stabilises viral and cellular mRNA transcripts

Having confirmed the interaction between RBM3 and NP mRNA, we next sought to identify how this interaction positively regulates WSN replication. Previous reports have suggested that RBM3 may stabilise certain bound transcripts in neuronal cells (20,21). Given this context, we next explored the stability of a subset of viral transcripts in the A549-RBM3+ or empty vector A549 cells. Cells were infected with WSN at an MOI 3 for 6 h, then treated with

247 actinomycin D to prevent further cellular and viral transcription (27). Transcript levels were
248 quantified hourly over 5 timepoints from 0-4 h post-actinomycin D treatment. The data were
249 plotted to visualise the decay of RNA over this treatment period (Figure 4), with a one-phase
250 decay model fitted to the data using a least squares regression. Observed differences in RNA
251 stability were significantly different between cell lines and were assessed by comparing the
252 decay constant (k) values using an extra sum-of-squares F test, with $p<0.05$ deemed
253 significant. Although no significant effect on the stability of viral HA mRNA was observed
254 (Figure 4A), a clear and significant increase in stability was quantified for NP mRNA with a
255 >70% increase in RNA half-life (Figure 4B). While viral M2 mRNA showed a modest increase
256 in half-life but no significant difference in stability (Figure 4C), it is noteworthy that
257 overexpression of RBM3 significantly and positively regulated cellular GAPDH levels (Figure
258 4D). This suggests that RBM3 stabilises mRNA transcripts, likely a form of cellular post-
259 transcriptional regulation for transcripts such as GAPDH, YAP1 (20) or GAS6 (21). This
260 mechanism is seemingly exploited by IAV during infection to promote viral transcript stability
261 and overall viral replication.

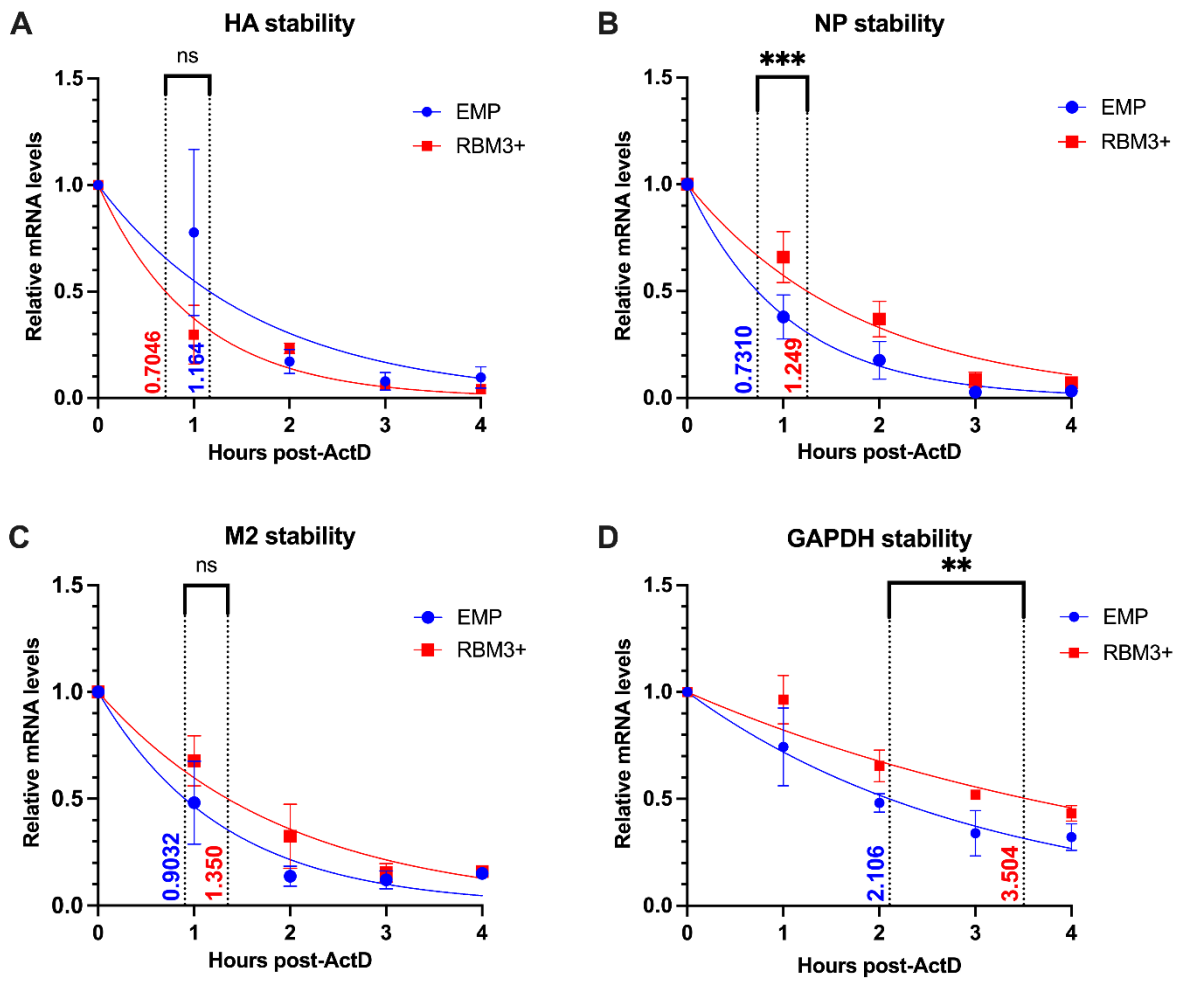

262

263 *Figure 4 – Binding of RBM3 has a stabilising effect on mRNA transcripts.*

264 *Transcript stability in empty vector or RBM3 overexpression A549 cells was established by an actinomycin D (ActD) assay*
265 *commenced at 6 hpi. Viral transcripts HA **(A)**, NP **(B)** and M2 **(C)**, and the cellular transcript GAPDH **(D)** were quantified over*
266 *5 hours with transcript half-lives quantified by a one-phase decay using a least squares regression.*

267 An RNA-binding null RBM3 and a tethering reporter system confirms the stabilisation of

268 RBM3-bound transcripts

269 RBM3 is composed of two major domains; an RNA Recognition Motif (RRM) found at the C-

270 terminus, and an N-terminus arginine-glycine rich (RGG) domain (Figure 5A) (28). The former

271 contains two highly conserved RNA binding regions, RNP2 and RNP1. After establishing the

272 binding between NP mRNA and RBM3, we proceeded to investigate how an RNA-binding null

273 mutant RBM3 would affect viral replication. We hypothesised that any pro-viral function

274 would be lost through ablation of RNA-binding. To test this, we created an RBM3 RNA-binding

275 null mutant cell-line, in which mutations were introduced to substitute phenylalanine (F)
276 residues within RNP2 and RNP1 to leucine (L) (Figure 5A). Previous studies have shown that
277 single L>F substitutions within RNP motifs disrupt the RNA binding ability (29). When viral
278 titres from infected A549-RBM3+ and A549-RBM3 mutant cell lines were compared (Figure
279 5B), we observed a significant >95% decrease in titres from the RBM3 mutant cells.
280 Actinomycin D assays to determine RNA stability were repeated in A549-RBM3+ and RBM3
281 mutant cell lines. These revealed a loss of the stabilisation phenotype in the RBM3 mutant
282 cells for viral NP transcripts as well as cellular GAPDH (Figure 5C and 5D). Interestingly, a 70%
283 decrease in half-life for NP mRNA in the RBM3 mutant cells was observed, mimicking the
284 phenotype observed in the A549-EMP cells. These results indicate that, through mutation of
285 the RNA-binding motifs of RBM3 to generate an RNA-binding null mutant, we can obviate the
286 stabilisation capacity of RBM3, consequently leading to a decrease in virus output.

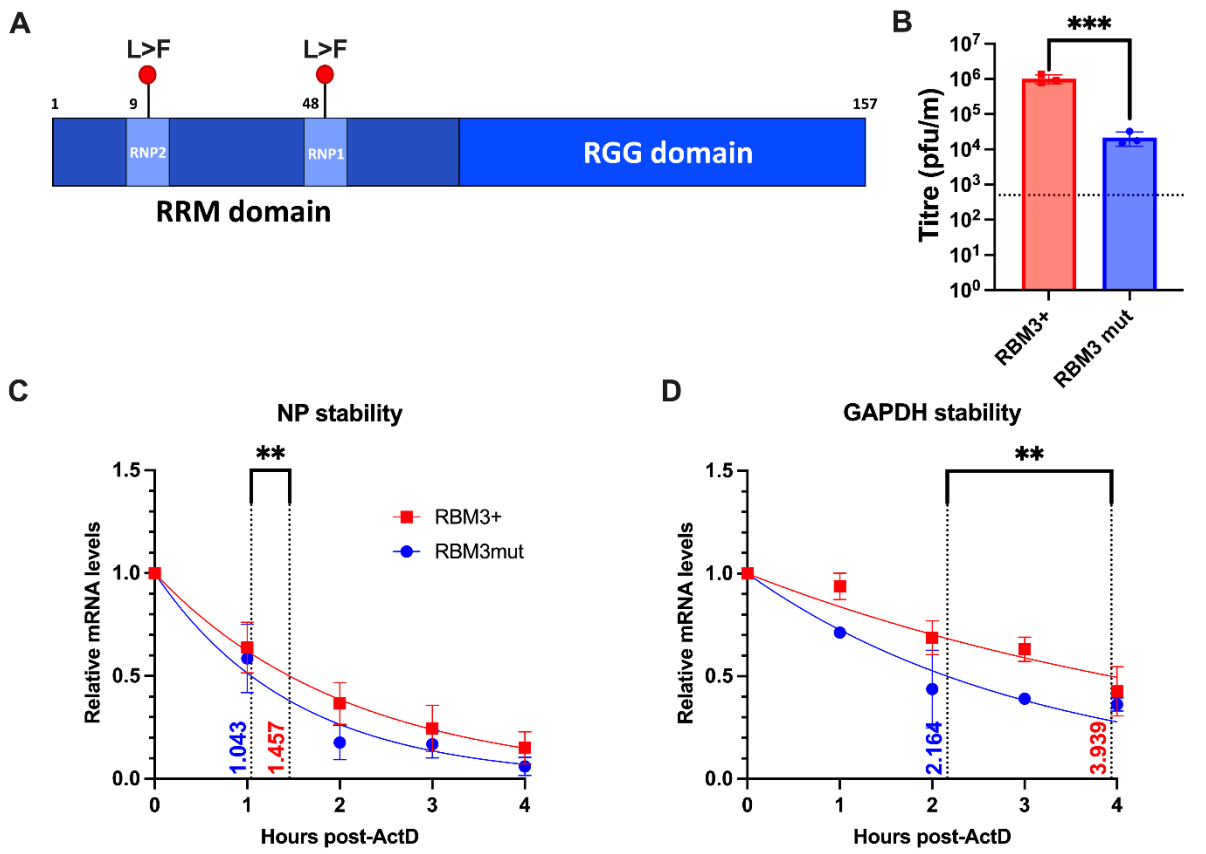

Figure 5 – Stability of mRNAs conferred by the overexpression of RBM3 is lost upon mutagenesis of the RNA-binding domains.

Schematic representation of RBM3. Single nonsense mutations were introduced into the RNA binding domains, RNP2 and RNP1, creating an RNA-binding null mutant RBM3. ***(B)*** *A549-RBM3+ or A549-RBM3 mut cells were infected at MOI 0.01 with WSN for 48 hours. Supernatants were harvested and titrated. Dotted line indicates the limit of detection.* ***(C,D)*** *A549-RBM3+ or A549-RBM3 mut cells were infected with MOI 3 WSN for 6 hours, then treated with ActD. Viral NP transcripts (C) and cellular GAPDH (D) were quantified over 4 hours with transcript half-lives quantified by a one-phase decay using a least squares regression.*

Although our half-life experiments suggest a role for RBM3 as a NP mRNA stabilising agent, we wanted to be certain of this function using a minimalist tethering experiment. To accomplish this, we set up a reporter system in which 293T cells were transfected with a Renilla Luciferase encoding for BoxB hairpins in the 3' UTR, and either WT RBM3 or LambdaN (λN)-RBM3 fusion protein (Figure 6A). The 19 nt BoxB hairpin acts as the target sequence for λN binding and fusion of λN with an RNA-binding protein allows for elucidation of the RBP's function on the BoxB-encoded reporter RNA (30). Actinomycin D assays were repeated 48 hours post-transfection and levels of luciferase RNA were assessed by qPCR. A significant enhancement in transcript half-life was observed upon expression of the fused λN-RBM3

304 protein (Figure 6B), providing further evidence that supports the role of RBM3 as an mRNA

305 stabilising agent.

306

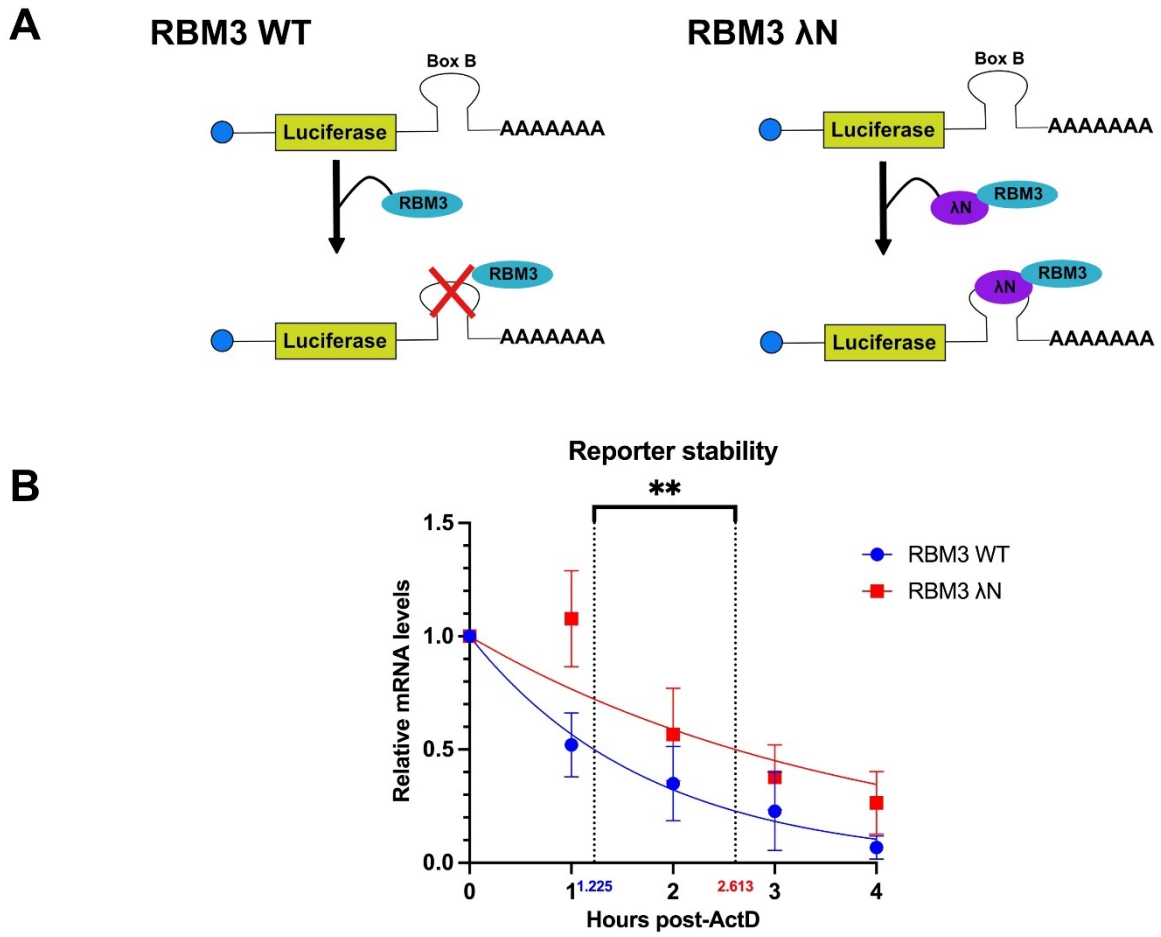

307

308 *Figure 6 – Confirmation of RBM3 as a stabilising agent using a tethering function assay.*

309 **(A)** *Schematic representation of the tethering reporter assay.* ***(B)*** *293T cells were transfected with a Luciferase BoxB reporter*
310 *alongside either WT RBM3 or fused λN-RBM3. Cells were treated with Act D 48 hours post-transfection. Luciferase transcripts*
311 *were quantified over 4 hours with transcript half-lives quantified by a one-phase decay using a least squares regression.*

312 <u>ASO-mediated increase of RBM3 levels in primary cells promotes overall viral replication</u>

313 Finally, we wanted to determine whether RBM3-mediated increase of overall viral replication

314 would be mirrored in PNECs. Previous studies have determined that targeted ASO treatment

315 of the RBM3 poison exon Ex3a in immortalised cell lines can result in the exclusion of the

316 poison exon, preventing NMD of RBM3 transcripts, and thus increasing overall RBM3 levels,

317 effectively mimicking the function of HNRNPH1 (24). Treatment of A549 cells with this
318 previously published Ex3a-specific ASO for 48 h resulted in an almost 4-fold increase in RBM3
319 transcript levels compared to that of a non-targeting control (Figure 7A), confirming its
320 effectiveness. Next, ASO treatment was applied apically to PNEC cultures from 3 donors.
321 Primary cells are much less permissive to transfection, therefore, ASO treatment would be
322 predicted to be much less effective at inducing RBM3 in these cultures. Nevertheless, we
323 observed a robust and significant ~50% increase in RBM3 transcript levels after 48 h
324 compared to the control ASO for all 3 donors (Figure 7B). Following this, we subjected PNEC
325 cultures from the same 3 donors to ASO treatment followed by infection with WSN for 48 h.
326 We then evaluated viral replication in these PNECS by quantification of viral RNA levels at 48
327 hpi. A significant increase in both NP mRNA and vRNA levels was observed by qPCR for each
328 donor upon treatment with the Ex3A-specific ASO, with mRNA levels on average more than
329 doubling after Ex3a ASO treatment (Figure 7C). These data confirm our earlier observations
330 that increasing RBM3 levels positively regulates IAV replication, in a highly relevant human
331 respiratory epithelial model of infection.

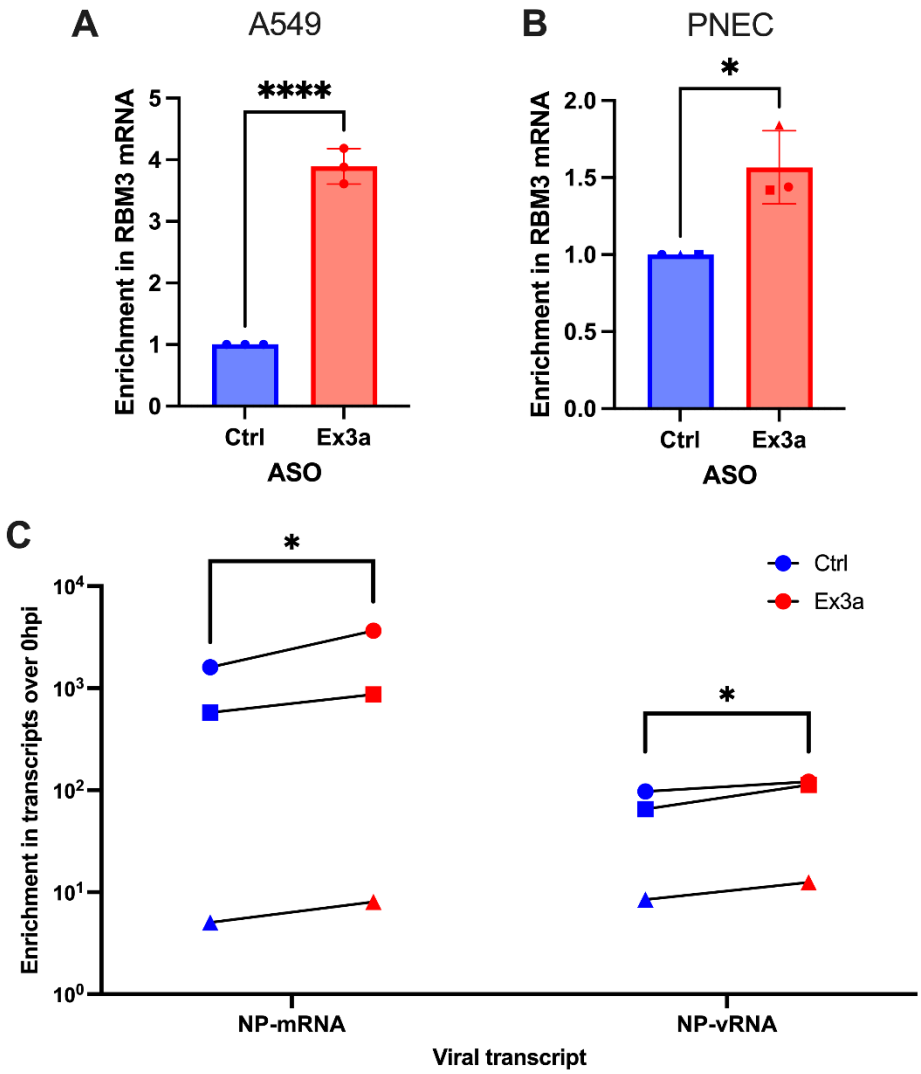

332

333 *Figure 7 - Increasing expression of RBM3 in PNECs significantly increases IAV replication*

334 ***(A)*** *Control (Ctrl) or Exon3a (Ex3a) specific ASOs were initially tested in A549 cells to determine their effectiveness in increasing*
335 *overall RBM3 mRNA levels, with an approximate 4-fold increase observed at 48 h post-transfection.* ***(B)*** *This was replicated*
336 *in PNECs at 48 h post-transfection where an approximate 50% ASO-mediated increase in RBM3 levels was quantified.* ***(C)***
337 *Quantifying viral mRNA and vRNA production in 3 donors (indicated by different shaped data points) previously treated with*
338 *Ctrl or Ex3a ASOs, demonstrated a significant increase in overall viral replication at 48 hpi.*

339

340 ## Discussion

341 Considering the persistent threat of a respiratory virus pandemic, whether that be another
342 coronavirus as seen with SARS-CoV-2, or a novel influenza strain such as the avian H5N1
343 circulating globally in wildlife, a thorough understanding of the tissues in which these viruses
344 replicate is critical to combat potential pandemic risk. The URT serves as an important tissue
345 for understanding the transmission of these respiratory virus. To prevent onward
346 transmission, it is critical to limit viral replication and shedding from the URT (7). Therefore,
347 there is a need to better characterise the cell biology of the URT, specifically the
348 nasopharyngeal epithelium, to uncover unique virus-host interactions that may be essential
349 for viral replication. Given the nasopharyngeal tissue of the URT is cooler than conventional
350 core body temperature of around 37°C, it is likely that this reduction in temperature will have
351 substantial effects on cell biology, resulting in important mechanistic differences in viral
352 replication.

353 Herein, we uncovered how the overall environment of mRNA-binding proteins is altered in
354 A549 cells cultured at 33°C compared to 37°C (Figure 1), and investigated how this would
355 affect IAV replication. While we identified 63 RBPs unique to our 33°C dataset and 151 unique
356 to our 37°C dataset, there were 209 RBPs in common between both growth temperatures.
357 RBM3 was one such factor, shown to be significantly enriched on mRNAs at 33°C compared
358 to 37°C. RBM3 is a known cold-inducible protein that has recently been shown to be regulated
359 by the binding efficiency of HNRNPH1 to a poison exon (13). Studies have uncovered a role
360 for RBM3 in promoting cell survival during cold stress (31,32), which may be due to positive
361 regulation of post-transcriptional processes including mRNA stability (20,21) and translation
362 (33). Aside from RBM3, several of the most enriched RBPs we observed in the 33°C RBPome,

363 including SND1, HNRNPC, TIA1 and ZC3H11A, have previously been reported to directly
364 associate with and regulate the RNAs of multiple respiratory viruses. SND1 has been reported
365 to associate with SARS-CoV-2 negative-sense RNA, with its binding required for viral RNA
366 synthesis (19). HNRNPC and TIA1 have also been identified as important SARS-CoV-2 RNA
367 binders, both promoting overall virus replication (34,35). Additionally, ZC3H11A has been
368 shown to positively regulate polyadenylation of HAdV-5 viral transcripts (36) and a further
369 cold-enriched RBP, YBOX1, may direct IAV vRNPs to the microtubule organising centre
370 (MTOC) (37).

371 Furthermore, RBM47 was found to be enriched over 3.5-fold in the 33°C dataset over that of
372 the 37°C. RBM47 is a broadly anti-viral RBP that has been shown to increase in expression in
373 the presence of viral infection or IFN stimulation and is essential for enhancing host IFN
374 signalling (38). Given that we have identified a greater level of RBM47 on cellular mRNAs at
375 33°C, it is interesting to speculate what role this may play in the baseline innate immune
376 responses of nasopharyngeal epithelial cells. If the increased abundance of RBM47 on host
377 mRNAs leads to a more anti-viral environment through enhancement of IFN signalling, then
378 RBM47 may be an important factor for our understanding of viral replication kinetics in the
379 URT and warrants further investigation.

380 With strong evidence that RBM3 is highly expressed in the URT (39), positively regulates
381 bound RNAs (20,21), and may bind to IAV NP mRNAs (22), we investigated how RBM3 directly
382 affects IAV replication. Knockdown of RBM3 resulted in a significant reduction in viral tires
383 and mRNA production (Figure 2). However, this is not necessarily indicative of a direct
384 interaction between RBM3 and viral mRNAs. Through a combination of RBPmap prediction
385 (25) of RBM3 binding motifs within WSN transcripts and CLIP-qPCR, we confirmed that RBM3
386 directly interacts with at least the NP mRNA of WSN (Figure 3). We next investigated how NP

387 mRNA may be affected by RBM3 binding. Recent studies identified RBM3 as a likely stabilising
388 factor for YAP1 (20) and GAS6 (21) transcripts, thus we investigated the stability of viral
389 mRNAs in our RBM3 overexpressing A549 cell line (Figure 4). We observed a significantly
390 elongated degradation profile for NP mRNA when RBM3 was overexpressed, but this was lost
391 upon mutagenesis of the RNA-binding domains of RBM3. We confirmed this phenotype in an
392 RBM3 tethering experiment, finding that recruitment of RBM3 to the 3'UTR of a reporter
393 mRNA significantly increased RNA half-life (Figure 5). Finally, to validate whether this
394 phenotype translates to a more clinically relevant model of IAV infection, we used a targeted
395 ASO treatment to increase RBM3 expression in primary nasal epithelial cells, prior to
396 infection. While there was the expected donor-to-donor variability in infection levels, overall
397 higher levels of RBM3 expression in each donor had a significant effect on multicycle viral
398 replication, quantified by increases in both NP mRNA and vRNA levels (Figure 6).

399 From these data, it is clear that the increased levels of RBM3 found in the nasopharyngeal
400 tissue of the URT would provide a pro-viral environment for IAV replication and transmission.
401 However, it remains to be determined if this would extend to the positive regulation of other
402 respiratory viruses. We have shown that RBM3 directly binds to IAV transcripts, with a
403 particular focus on NP mRNA. As RBM3 clearly increases the stability of NP mRNA, it is
404 incumbent to further investigate how cooler temperatures affect more general aspects of
405 RNA biology. Some cellular processes slow down due to cooler growth temperatures, with
406 translation rates being a key process among those reported to measurably decline (33).
407 Consequently, mature mRNAs would have to reside in the cell longer to be efficiently
408 translated. It is worth speculating that the stabilising role for RBM3 may then be in directly
409 preventing bound mRNAs from degradation by nucleases. This may be through protecting the
410 bound mRNA from endonuclease recognition and cleavage, or inhibiting binding of decay

411 factors, such as the exosome complex (40). Alternatively, Dresios et al., have reported that
412 overexpression of RBM3 enhances protein synthesis of targeted genes (33). As stated earlier,
413 it is well known that cooler growth conditions inhibit protein synthesis. Therefore, if RBM3
414 increases the ribosome loading of bound transcripts, the protection conferred by the
415 translation machinery would positively regulate transcript half-life. However, it cannot be
416 discounted that stability stemming from RBM3 binding may arise from stabilisation of RNA
417 secondary structures shown to be important for viral RNAs (41), modulation of RNA
418 modifications which are known to affect IAV transcripts (42), or even sequestration of mRNA
419 into membraneless organelles, already known to be important during vRNA trafficking (43).
420 While it appears IAV has evolved to recruit RBM3 to NP mRNA to positively regulate transcript
421 stability, and by extension overall IAV replication, we should also consider that this
422 mechanism of action may be hijacked for therapeutic purposes. With the seemingly rapid,
423 and successful deployment of mRNA vaccines to combat severe pathology arising from a
424 pandemic respiratory virus (44), in SARS-CoV-2, the next potential avenue in pandemic
425 preparedness would be the development of nasal vaccines that can induce a robust IgA
426 response and prevent onward transmission from the URT (45,46). With an inhalable form of
427 mRNA therapeutic having recently been successfully delivered to the airways of mice (6), it is
428 perhaps pertinent to explore whether the mRNA stabilising effects of RBM3 may be exploited
429 to enhance such therapies in the future.
430 Herein, we present RBM3 as an important host factor for IAV replication in the URT. RBM3 is
431 highly expressed in the nasopharyngeal tract due to cooler growth temperatures influenced
432 by the external environment. RBM3 binds to and stabilises IAV NP mRNA, while its loss has a
433 significantly inhibitory effect on viral replication. Taken together, it is clear that RBM3 is an

434 important host factor for efficient replication and onward transmission of IAV from the
435 nasopharyngeal tract.

436 **Methods**

437 Cells

438 All immortalised cell lines were cultured in DMEM supplemented with 1% Pen-Strep (Thermo
439 Fisher Scientific; 15140122) and 5% FBS (Thermo Fisher Scientific; 10270106) at 37°C/33°C
440 and 5% CO_2. Cell lines used were A549s (ATCC; CCL-185), HEK 293Ts (ATCC; CRL-3216), MDCKs
441 (CCL-34), Hep2s (ATCC; CCL-23), HeLa H1s (ATCC; CRL-1958), Beas2Bs (ATCC; CRL-3588), RPMI
442 2650s (ATCC; CCL-30) and Calu3s (ATCC; HTB-55).

443 Virus stocks and infections

444 IAV WSN (A/WSN/33) stocks were generated from a reverse genetics system previously
445 described (47). WSN stocks were grown on MDCK cells in IAV growth media consisting of
446 DMEM, Pen-Strep, 0.2% BSA (Merck; A8412), 25mM HEPES (Merck; H0887) and TPCK-trypsin
447 (Merck; T8802) and titrated on MDCK cells by plaque assay.

448 RIC

449 The protocol employed here to capture the RNA interactome of poly(A)+ RNA (RIC) from A549
450 cells has been described previously (17,23). However, we made one minor modification. At
451 the time of seeding, 48 h before crosslinking and harvesting, A549 cells were either incubated
452 under the normal growth temperature of 37°C, to determine the 37°C RBPome, or incubated
453 in a 33°C incubator, to determine the 33°C RBPome. Cells were grown for 48 h at these
454 conditions before performing UV crosslinking at 254nm and lysis. The remaining steps were
455 followed exactly as has been described previously (23).

456 Protein visualisation

457 Western blotting was performed as has been previously described (48). Primary antibodies
458 for influenza PA (Thermo Fisher Scientific; Pa5-32223), RBM3 (Proteintech; 14363-1-AP),
459 ACTB (Proteintech; 66009-1-ig), and Flag (Proteintech; 66008-3-ig) were all used at a 1:5000
460 dilution. Proteins bands on blots were visualised by chemiluminescence. Total protein was
461 imaged by silver staining (Thermo Fisher Scientific; 24612), following the manufacturer's
462 protocol.

463 LC-MS/MS and data analysis

464 Mass spectrometry of RIC samples was performed at the Cambridge Centre for Proteomics.
465 Sample treatment, preparation and trypsin digestion were performed as described previously
466 (49). Data for each sample were acquired on an Orbitrap Fusion Lumos Tribrid mass
467 spectrometer over a 60 min run. No fractionation was performed due to the likely low
468 complexity of the sample. Raw mass spectrometry data was analysed using MaxQuant
469 software (v2.4.7.0) and utilising the Andromeda search engine (50). The MS/MS spectra were
470 aligned to the Uniprot Homo sapiens protein database, with known mass spectrometry
471 contaminants and reversed sequences also included. The search was performed with trypsin
472 selected as the specific enzyme and a maximum of 2 missed cleavage events allowed. The MS
473 accuracy was set to 10 ppm, then 0.05 Da for the MS/MS. The maximum peptide charge was
474 set to seven and seven amino acids were required for the minimum peptide length. One
475 unique peptide to the protein group was required to call the presence of a specific protein,
476 while a false-discovery rate (FDR) of 1% was set. Statistical analysis to determine enriched
477 proteins in one set of biological samples over another was performed using the intensities
478 quantified by MaxQuant on Perseus software (v2.0.11) (51). First, any potential contaminants,
479 reverse hits or proteins that were not well identified (fell below 1% FDR) were removed. Then

480 only proteins that were identified in at least 2 replicates from a single biological condition
481 were utilised. After filtering, the intensities were log transformed (log_2) and statistical
482 significance was calculated by way of an unpaired two-tailed Student's t-test for each protein
483 group. These values were then log transformed ($-log_{10}$) and the resulting p values and
484 enrichments were graphed as volcano plots. The cutoff for statistical significance was set to
485 $p < 0.05$.

486 siRNA knockdowns

487 A pair of siRNAs targeting the specified mRNA were used in each knockdown experiment,
488 aside from when a single non-specific control siRNA (siNSC) was used. Sequences of these
489 siRNAs are listed in Supplementary Table 3. A final concentration of 20nM total siRNA was
490 used, and these were transfected using Lipofectamine RNAiMAX (Invitrogen; 13778075)
491 following the manufacturer's instructions. A549 cells were seeded and transfected
492 simultaneously and incubated for 24 h, after which media was changed with fresh growth
493 media. Cells were then incubated for a further 24 h prior to infection.

494 Establishment of a RBM3 overexpression cell line using a lentiviral vector

495 A lentiviral expression plasmid was generated encoding for either a full length wild-type RBM3
496 C-terminally tagged with 2X Flag epitope tags (RBM3+), a full-length RNA-binding mutant
497 (RBM3-Mut), containing two single phenylalanine to leucine substitutions within RNP1 (L48F)
498 and RNP2 (L9F), or an empty vector (A549-EMP). A549-RBM3, A549-EMP and A549-Mut were
499 followed by a P2A self-cleaving peptide and a puromycin resistance gene, similar to a system
500 we have published previously (42). Again, similar to previous publications, we rescued
501 lentiviral particles by co-transfecting 293T cells with the RBM3, RBM3 Mut or EMP lentiviral
502 vector alongside d8.74 (Addgene; 22036) and MD2G (Addgene; 12259). At 72 h post-

503 transfection the supernatant was harvested, passed through a 0.45 μm filter and then
504 overlaid onto fresh A549 cells. At 72 h post transduction cells were treated with 2 μg/ml
505 puromycin and left to select for 72 h. Cells were then single cell cloned in 96 well plates in the
506 presence of 2 μg/ml puromycin and left to grow for 3 weeks. Single cell colonies were then
507 selected, expanded, and checked by Western blot to confirm the expression of the transgene.

508 CLIP-qPCR

509 The CLIP-qPCR protocol employed here has been published previously (52). Briefly, A549-
510 RBM3 and A549-EMP cells were seeded one day prior to infection. Cells were infected with
511 A/WSN/33 at an MOI 3 PFU/cell and incubated for 6 h. At 6 hpi media was removed from the
512 cells, before being washed in ice cold PBS. UV crosslinking was performed at 254nm. Cells
513 were then scraped, pelleted and lysed in 250 µl of NP40 lysis buffer (HEPES-KOH pH 7.5
514 50mM, KCl 150mM, EDTA pH 8.0 2mM, NaF 1mM and NP40 0.5%) on ice for 30 min. Lysates
515 were clarified by centrifugation and 10% of the sample was saved as an input and boiled in
516 Laemmli buffer containing 2% β-mercaptoethanol at 95°C for 10 min for western blotting. The
517 remaining 90% of lysate underwent immunoprecipitation with anti-Flag antibody (Merck,
518 F1804) coupled to Protein G Dynabeads (ThermoFisher, 10004D) for 1 h at room temperature.
519 Beads were then captured, washed five times with 1 mL NP40 lysis buffer and three times
520 with PBS. A fraction (10%) of the beads was removed, resuspended in Laemmli buffer and
521 boiled at 95°C for 10 min for Western blotting. The remaining 90% of beads underwent
522 proteinase K digestion (ThermoFisher, EO0491) at 55°C for 60 min to release bound RNA,
523 following the manufacturer's instructions. RNA was then isolated from the digestion by TRIzol
524 LS (ThermoFisher, 10296028) and ethanol precipitation and cDNA were synthesized using
525 oligo dT or A/WSN/33 specific primers (53) (Supplementary Table 4). Quantification of the

526 cDNAs was performed by qPCR, as described below. Fold enrichment of RNA levels was
527 quantified using the ΔΔCT method and normalised to input levels.

528 IAV growth kinetics at 37°C and 33°C

529 For multicycle IAV infections, A549 cells were seeded 48hrs before infection. Cells were
530 infected with A/WSN/33 at an MOI 0.01 PFU/cell in DMEM for 1 h. The inoculum was then
531 removed, and cells incubated for 48 h in IAV growth media, described above, supplemented
532 with TPCK-trypsin. Supernatants were then titrated on MDCK cells by plaque assay.

533 IAV qPCR growth curves

534 A549 cells were infected with A/WSN/33 virus at an MOI 0.01 PFU/cell. At 0, 8, 24 and 48 hpi
535 RNA was extracted from cells using TRIzol (Invitrogen; 15596026). RNA was isolated and
536 precipitated following the manufacturer's instructions and 200ng was reverse transcribed
537 into cDNA using the ABI cDNA synthesis kit (Applied Biosystems; 4368814). For all cellular
538 targets RT was performed using an oligo dT, while viral RNA underwent separate RT reactions
539 with primers specific to each mRNA or vRNA (53). These primers are listed in Supplementary
540 Table 4 alongside the primers used for qPCR amplification. All qPCR experiments were
541 performed using SYBR Select Master Mix (Applied Biosystems; 4472908) following the
542 manufacturer's instructions. All qPCR data were quantified using the ΔΔCT method.

543 Actinomycin D assays

544 A549-RBM3+, A549-Mut and A549-EMP cells were seeded at a density of 1 x 10^5 cells/well
545 one day prior to infection. Cells were infected with WSN at a MOI of 3 PFU/cell. At 6 hpi, RNA
546 was harvested from a single well for each cell type, constituting the 0 h timepoint. All
547 remaining infected wells underwent media exchange for growth media containing containing
548 2 µg/mL Actinomycin D (SBR00013). RNA was harvested hourly from 7-10 hpi representing 1-

549 4 h post Actinomycin D treatment. RNA underwent cDNA conversion using oligo dT or
550 A/WSN/33 specific primers, with the ABI cDNA synthesis kit (Applied Biosystems; 4368814).
551 Quantification of the cDNAs was performed by qPCR, described above. Fold enrichment of
552 RNA levels was quantified using the ΔΔCT method and normalised to either A549-EMP or
553 A549-RBM3 levels.

554 λN tethering assay

555 λN was cloned into a lentiviral expression vector expressing full-length WT RBM3. 293T cells
556 were seeded at a density of 1 x 10^5 cells/mL in a 12-well plate the day before transfection.
557 The following day, cells were transfected with 500 ng of pCI-RLuc-BoxB and 100 ng of either
558 the WT RBM3 or the λN-RBM3 WT expressing plasmids. At 48 hours post-transfection, RNA
559 was harvested from a single well for each transfection to represent a 0h timepoint. All
560 remaining cells were treated with 2 µg/mL Actinomycin D (SBR00013). RNA was harvested by
561 TRIzol hourly up to 4 hours post-treatment. RNA underwent DNaseI (Invitrogen, EN0521)
562 digestion to remove any residual plasmid DNA before cDNA conversion using oligo dT primers
563 with the ABI cDNA synthesis kit (Applied Biosystems; 4368814). Quantification of the cDNAs
564 was performed by qPCR, described above. Fold enrichment of luciferase RNA levels was
565 quantified using the ΔΔCT method and normalised to the corresponding 0 h mRNA levels.

566 Well-Differentiated Primary Airway Epithelial Cell Culture

567 Primary nasal epithelial cells were obtained from Promocell and well differentiated primary
568 nasal epithelial cell (WD-PNEC) cultures were established as described previously (54). Briefly,
569 WD-PNECs were seeded onto collagen coated 6 mm Transwells (Sarstedt, 83.3932.041) at
570 3x10^4 cells/transwell. Cells were submerged in modified Promocell Airway Epithelial Cell
571 Growth Medium which was replaced on the apical and basal side every 2 days until the cells

572 reached confluency. Once confluent, an air liquid interface (ALI) was initiated by completely
573 removing the apical medium. Cells were differentiated using Pneumacult ALI medium
574 (Stemcell Technologies, #05001) supplemented with hydrocortisone and heparin. For
575 downstream experiments, WD-PNECs were only used when there was extensive cilia
576 coverage and mucus production, clear hallmarks of full differentiation.

577 ASO transfection and IAV infection of cells

578 A549s were transfected with control or Exon 3a targeting ASOs (24) (Supplementary Table 5)
579 to initially test whether induction of RBM3 could be achieved in airway cells. ASOs were
580 resuspended in DMEM at a concentration of 1 µM and transfected using Lipofectamine 2000
581 (Invitrogen, 1 µL/mL). At 48 h post-transfection RNA was harvested, cDNA synthesised as
582 described above, and RBM3 levels quantified by qPCR. For WD-PNEC cells, the transfection
583 conditions were the same, with the ASO-containing transfection mix added apically to WD-
584 PNECs. Cells were incubated for 48 h prior to infection with WSN MOI 0.01 PFU/cell in DMEM.
585 At 1 hpi, the inoculum was removed and transwells were washed 5 times in DMEM to remove
586 unbound virus. RNA was harvested from WD-PNECS using Trizol™ either before infection or
587 at 72 hours post-infection.

588 Statistical analysis

589 Unless otherwise stated, all experiments were performed as 3 independent biological
590 replicates. When bar graphs are used to represent the data, each individual replicate can be
591 observed as a point overlaid on the bar, with error bars indicating standard deviation.
592 Significance was calculated by performing Student's t-test with * indicating $p<0.05$, **
593 indicating $p<0.01$ and *** indicating $p<0.001$.

Acknowledgements

This research was funded in part by an ERC-STG grant, PTFLU 949506 awarded to D.G.C. This research received infrastructure support from the Wellcome-Wolfson Institute for Experimental Medicine at Queen's University Belfast.

In Figure 1 cells_bilayer icon by Marcel Tisch is licensed under CC0, upper-respiratory-tract icon by Servier https://smart.servier.com/ is licensed under CC-BY 3.0 Unported, lung icon by Servier https://smart.servier.com/ is licensed under CC-BY 3.0 Unported, all protein icons by Servier https://smart.servier.com/ is licensed under CC-BY 3.0 Unported, Liquid_Chromatograph_Mass_Spectrometer icon by DBCLS https://togotv.dbcls.jp/en/pics.html is licensed under CC-BY 4.0 Unported and rna icon by Servier https://smart.servier.com/ is licensed under CC-BY 3.0 Unported.

607 **References**

608 1. Lakdawala SS, Jayaraman A, Halpin RA, Lamirande EW, Shih AR, Stockwell TB, et
609 al. The soft palate is an important site of adaptation for transmissible influenza
610 viruses. Nature [Internet]. 2015 Sep 23 [cited 2024 Jul 17];526(7571):122–5.
611 Available from: https://www.nature.com/articles/nature15379

612 2. Xie C, Su W, Sia SF, Choy KT, Morrell S, Zhou J, et al. A(H1N1)pdm09 Influenza
613 Viruses Replicating in Ferret Upper or Lower Respiratory Tract Differed in
614 Onward Transmission Potential by Air. J Infect Dis [Internet]. 2022 Jan 1 [cited
615 2023 Oct 26];225(1):65–74. Available from:
616 https://pubmed.ncbi.nlm.nih.gov/34036370/

617 3. Richard M, van den Brand JMA, Bestebroer TM, Lexmond P, de Meulder D,
618 Fouchier RAM, et al. Influenza A viruses are transmitted via the air from the nasal
619 respiratory epithelium of ferrets. Nature Communications 2020 11:1 [Internet].
620 2020 Feb 7 [cited 2023 Nov 14];11(1):1–11. Available from:
621 https://www.nature.com/articles/s41467-020-14626-0

622 4. Varble A, Albrecht RA, Backes S, Crumiller M, Bouvier NM, Sachs D, et al.
623 Influenza A Virus Transmission Bottlenecks Are Defined by Infection Route and
624 Recipient Host. Cell Host Microbe. 2014 Nov 12;16(5):691–700.

625 5. Bisht K, te Velthuis AJW. Decoding the Role of Temperature in RNA Virus
626 Infections. mBio [Internet]. 2022 Sep 1 [cited 2023 Oct 26];13(5). Available from:
627 https://journals.asm.org/doi/10.1128/mbio.02021-22

628 6. Suberi A, Grun MK, Mao T, Israelow B, Reschke M, Grundler J, et al. Polymer
629 nanoparticles deliver mRNA to the lung for mucosal vaccination. Sci Transl Med

630 [Internet]. 2023 Aug 16 [cited 2024 Jul 22];15(709). Available from:
631 https://www.science.org/doi/10.1126/scitranslmed.abq0603

632 7. McMahan K, Wegmann F, Aid M, Sciacca M, Liu J, Hachmann NP, et al. Mucosal
633 boosting enhances vaccine protection against SARS-CoV-2 in macaques. Nature
634 2023 626:7998 [Internet]. 2023 Dec 14 [cited 2024 Jul 8];626(7998):385–91.
635 Available from: https://www.nature.com/articles/s41586-023-06951-3

636 8. Eccles R. Why is temperature sensitivity important for the success of common
637 respiratory viruses? Rev Med Virol [Internet]. 2021 Jan 1 [cited 2023 Nov
638 19];31(1):1–8. Available from: /pmc/articles/PMC7435572/

639 9. Otter CJ, Fausto A, Tan LH, Khosla AS, Cohen NA, Weiss SR. Infection of primary
640 nasal epithelial cells differentiates among lethal and seasonal human
641 coronaviruses. Proc Natl Acad Sci U S A [Internet]. 2023 Apr 11 [cited 2023 Oct
642 26];120(15):e2218083120. Available from:
643 https://www.pnas.org/doi/abs/10.1073/pnas.2218083120

644 10. Pullara P, Alshareedah I, Banerjee PR. Temperature-dependent reentrant phase
645 transition of RNA-polycation mixtures. Soft Matter [Internet]. 2022 Feb 21 [cited
646 2023 Nov 1];18(7):1342–9. Available from:
647 https://pubmed.ncbi.nlm.nih.gov/34984429/

648 11. Riback JA, Katanski CD, Kear-Scott JL, Pilipenko E V., Rojek AE, Sosnick TR, et al.
649 Stress-Triggered Phase Separation Is an Adaptive, Evolutionarily Tuned
650 Response. Cell [Internet]. 2017 Mar 9 [cited 2023 Nov 1];168(6):1028-1040.e19.
651 Available from: https://pubmed.ncbi.nlm.nih.gov/28283059/

652 12. Tauber D, Tauber G, Parker R. Mechanisms and Regulation of RNA Condensation
653 in RNP Granule Formation. Trends Biochem Sci [Internet]. 2020 Sep 1 [cited 2023
654 Nov 1];45(9):764–78. Available from:
655 https://pubmed.ncbi.nlm.nih.gov/32475683/

656 13. Lin JQ, Khuperkar D, Pavlou S, Makarchuk S, Patikas N, Lee FC, et al. HNRNPH1
657 regulates the neuroprotective cold-shock protein RBM3 expression through
658 poison exon exclusion. EMBO J [Internet]. 2023 Jul 17 [cited 2023 Nov
659 1];42(14):e113168. Available from:
660 https://onlinelibrary.wiley.com/doi/full/10.15252/embj.2022113168

661 14. Cugusi S, Mitter R, Kelly GP, Walker J, Han Z, Pisano P, et al. Heat shock induces
662 premature transcript termination and reconfigures the human transcriptome.
663 Mol Cell [Internet]. 2022 Apr 21 [cited 2024 Jul 23];82(8):1573-1588.e10.
664 Available from: http://www.cell.com/article/S1097276522000077/fulltext

665 15. Gagnon D, Barry H, Barhdadi A, Oussaid E, Mongrain I, Lemieux Perreault LP, et
666 al. A dataset of proteomic changes during human heat stress and heat
667 acclimation. Scientific Data 2023 10:1 [Internet]. 2023 Dec 7 [cited 2024 Jul
668 23];10(1):1–6. Available from: https://www.nature.com/articles/s41597-023-
669 02809-5

670 16. Kamel W, Noerenberg M, Cerikan B, Chen H, Järvelin AI, Kammoun M, et al.
671 Global analysis of protein-RNA interactions in SARS-CoV-2 infected cells reveals
672 key regulators of infection. Mol Cell [Internet]. 2021 [cited 2021 May 25];
673 Available from: https://doi.org/10.1016/j.molcel.2021.05.023.

674 17. Garcia-Moreno M, Noerenberg M, Ni S, Järvelin AI, González-Almela E, Lenz CE,
675 et al. System-wide Profiling of RNA-Binding Proteins Uncovers Key Regulators of
676 Virus Infection. Mol Cell. 2019;74(1):196-211.e11.

677 18. Bonazza S, Coutts HL, Sukumar S, Turkington HL, Courtney DG. Identifying
678 cellular RNA-binding proteins during infection uncovers a role for MKRN2 in
679 influenza mRNA trafficking. Schwemmle M, editor. PLoS Pathog [Internet]. 2024
680 May 16 [cited 2024 May 20];20(5):e1012231. Available from:
681 https://dx.plos.org/10.1371/journal.ppat.1012231

682 19. Schmidt N, Ganskih S, Wei Y, Gabel A, Zielinski S, Keshishian H, et al. SND1 binds
683 SARS-CoV-2 negative-sense RNA and promotes viral RNA synthesis through
684 NSP9. Cell [Internet]. 2023 Oct 26 [cited 2024 Mar 28];186(22):4834-4850.e23.
685 Available from: https://pubmed.ncbi.nlm.nih.gov/37794589/

686 20. Xia W, Su L, Jiao J. Cold-induced protein RBM3 orchestrates neurogenesis via
687 modulating Yap mRNA stability in cold stress. J Cell Biol [Internet]. 2018 Oct 1
688 [cited 2023 Nov 1];217(10):3464–79. Available from:
689 https://pubmed.ncbi.nlm.nih.gov/30037926/

690 21. Lin P, Lin C, Diao L. RBM3 Ameliorates Acute Brain Injury-induced Inflammation
691 and Oxidative Stress by Stabilizing GAS6 mRNA Through Nrf2 Signaling Pathway.
692 Neuroscience [Internet]. 2024 May 24 [cited 2024 Jul 11];547:74–87. Available
693 from: https://pubmed.ncbi.nlm.nih.gov/38555015/

694 22. Dupont M, Krischuns T, Gianetto QG, Paisant S, Bonazza S, Brault JB, et al. The
695 RBPome of influenza A virus NP-mRNA reveals a role for TDP-43 in viral

696 replication. Nucleic Acids Res [Internet]. 2024 Apr 30 [cited 2024 Jul 11];52(12).
697 Available from: https://pubmed.ncbi.nlm.nih.gov/38686810/

698 23. Castello A, Fischer B, Eichelbaum K, Horos R, Beckmann BM, Strein C, et al.
699 Insights into RNA Biology from an Atlas of Mammalian mRNA-Binding Proteins.
700 Cell [Internet]. 2012;149(6):1393–406. Available from:
701 http://dx.doi.org/10.1016/j.cell.2012.04.031

702 24. Preußner M, Smith HL, Hughes D, Zhang M, Emmerichs A, Scalzitti S, et al. ASO
703 targeting RBM3 temperature-controlled poison exon splicing prevents
704 neurodegeneration in vivo . EMBO Mol Med [Internet]. 2023 May 8 [cited 2024
705 Jul 18];15(5). Available from:
706 https://www.embopress.org/doi/10.15252/emmm.202217157

707 25. Paz I, Kosti I, Ares M, Cline M, Mandel-Gutfreund Y. RBPmap: a web server for
708 mapping binding sites of RNA-binding proteins. Nucleic Acids Res [Internet].
709 2014 Jul 1 [cited 2024 Jul 18];42(Web Server issue). Available from:
710 https://pubmed.ncbi.nlm.nih.gov/24829458/

711 26. Liu Y, Hu W, Murakawa Y, Yin J, Wang G, Landthaler M, et al. Cold-induced RNA-
712 binding proteins regulate circadian gene expression by controlling alternative
713 polyadenylation. Scientific Reports 2013 3:1 [Internet]. 2013 Jun 24 [cited 2024
714 Jul 23];3(1):1–11. Available from: https://www.nature.com/articles/srep02054

715 27. Ratnadiwakara M, Änkö ML. mRNA Stability Assay Using transcription inhibition
716 by Actinomycin D in Mouse Pluripotent Stem Cells. Bio Protoc [Internet]. 2018
717 [cited 2024 Jul 25];8(21). Available from:
718 https://pubmed.ncbi.nlm.nih.gov/34532533/

719 28. RB Z, XL L, CY Z, DC Y. RNA binding motif protein 3: a potential biomarker in
720 cancer and therapeutic target in neuroprotection. Oncotarget [Internet]. 2017
721 [cited 2024 Jul 23];8(13). Available from:
722 https://pubmed.ncbi.nlm.nih.gov/28118608/

723 29. Serin G, Joseph G, Ghisolfi L, Bauzan M, Erard M, Amalric F, et al. Two RNA-
724 binding domains determine the RNA-binding specificity of nucleolin. J Biol Chem
725 [Internet]. 1997 May 16 [cited 2024 Jul 23];272(20):13109–16. Available from:
726 https://pubmed.ncbi.nlm.nih.gov/9148924/

727 30. Baron-Benhamou J, Gehring NH, Kulozik AE, Hentze MW. Using the λN peptide
728 to tether proteins to RNAs. In: mRNA Processing and Metabolism Methods in
729 Molecular Biology . Humana Press; 2004.

730 31. Peretti D, Bastide A, Radford H, Verity N, Molloy C, Martin MG, et al. RBM3
731 mediates structural plasticity and protective effects of cooling in
732 neurodegeneration. Nature [Internet]. 2015 Feb 12 [cited 2023 Nov
733 1];518(7538):236–9. Available from:
734 https://pubmed.ncbi.nlm.nih.gov/25607368/

735 32. Wellmann S, Truss M, Bruder E, Tornillo L, Zelmer A, Seeger K, et al. The RNA-
736 Binding Protein RBM3 Is Required for Cell Proliferation and Protects Against
737 Serum Deprivation-Induced Cell Death. Pediatric Research 2010 67:1 [Internet].
738 2010 [cited 2024 Jul 22];67(1):35–41. Available from:
739 https://www.nature.com/articles/pr20107

740 33. Dresios J, Aschrafi A, Owens GC, Vanderklish PW, Edelman GM, Mauro VP. Cold
741 stress-induced protein Rbm3 binds 60S ribosomal subunits, alter microRNA

742 levels, and enhances global protein synthesis. Proc Natl Acad Sci U S A [Internet].
743 2005 Feb 8 [cited 2024 Jul 22];102(6):1865–70. Available from:
744 https://www.pnas.org/doi/abs/10.1073/pnas.0409764102

745 34. Zhang D, Qiao L, Lei X, Dong X, Tong Y, Wang J, et al. Mutagenesis and structural
746 studies reveal the basis for the specific binding of SARS-CoV-2 SL3 RNA element
747 with human TIA1 protein. Nature Communications 2023 14:1 [Internet]. 2023
748 Jun 22 [cited 2024 Jul 5];14(1):1–12. Available from:
749 https://www.nature.com/articles/s41467-023-39410-8

750 35. Zhang X, Chu H, Chik KKH, Wen L, Shuai H, Yang D, et al. hnRNP C modulates
751 MERS-CoV and SARS-CoV-2 replication by governing the expression of a subset
752 of circRNAs and cognitive mRNAs. Emerg Microbes Infect [Internet]. 2022 [cited
753 2024 Jul 5];11(1):519. Available from: /pmc/articles/PMC8843244/

754 36. Kases K, Schubert E, Hajikhezri Z, Larsson M, Devi P, Darweesh M, et al. The RNA-
755 binding protein ZC3H11A interacts with the nuclear poly(A)-binding protein
756 PABPN1 and alters polyadenylation of viral transcripts. Journal of Biological
757 Chemistry [Internet]. 2023 Aug 1 [cited 2024 Jul 5];299(8):104959. Available
758 from: http://www.jbc.org/article/S0021925823019877/fulltext

759 37. Kawaguchi A, Matsumoto K, Nagata K. YB-1 Functions as a Porter To Lead
760 Influenza Virus Ribonucleoprotein Complexes to Microtubules. J Virol [Internet].
761 2012 Oct 15 [cited 2024 Jul 5];86(20):11086. Available from:
762 /pmc/articles/PMC3457152/

763 38. Wang K, Huang C, Jiang T, Chen Z, Xue M, Zhang Q, et al. RNA-binding protein
764 RBM47 stabilizes IFNAR1 mRNA to potentiate host antiviral activity. EMBO Rep

765 [Internet]. 2021 Aug 4 [cited 2024 Jul 5];22(8). Available from:
766 https://pubmed.ncbi.nlm.nih.gov/34160127/

767 39. Thul PJ, Akesson L, Wiking M, Mahdessian D, Geladaki A, Ait Blal H, et al. A
768 subcellular map of the human proteome. Science (1979) [Internet]. 2017 May
769 26 [cited 2023 Nov 1];356(6340). Available from:
770 https://www.science.org/doi/10.1126/science.aal3321

771 40. Schmid M, Jensen TH. The exosome: a multipurpose RNA-decay machine. Trends
772 Biochem Sci [Internet]. 2008 Oct 1 [cited 2024 Jul 23];33(10):501–10. Available
773 from: http://www.cell.com/article/S0968000408001837/fulltext

774 41. Yang R, Pan M, Guo J, Huang Y, Zhang QC, Deng T, et al. Mapping of the influenza
775 A virus genome RNA structure and interactions reveals essential elements of
776 viral replication. Cell Rep [Internet]. 2024 Mar 26 [cited 2024 Apr 29];43(3).
777 Available from: https://pubmed.ncbi.nlm.nih.gov/38416642/

778 42. Courtney DG, Kennedy EM, Dumm RE, Bogerd HP, Tsai K, Heaton NS, et al.
779 Epitranscriptomic Enhancement of Influenza A Virus Gene Expression and
780 Replication. Cell Host Microbe. 2017;22:377–86.

781 43. Vale-Costa S, Etibor TA, Brás D, Sousa AL, Ferreira M, Martins GG, et al. ATG9A
782 regulates the dissociation of recycling endosomes from microtubules to form
783 liquid influenza A virus inclusions. PLoS Biol [Internet]. 2023 Nov 1 [cited 2024
784 Apr 23];21(11):e3002290. Available from:
785 https://journals.plos.org/plosbiology/article?id=10.1371/journal.pbio.3002290

786 44. Morens DM, Taubenberger JK, Fauci AS. Rethinking next-generation vaccines for
787 coronaviruses, influenzaviruses, and other respiratory viruses. Cell Host Microbe

788 [Internet]. 2023 Jan 11 [cited 2024 Apr 1];31(1):146–57. Available from:
789 http://www.cell.com/article/S1931312822005728/fulltext

790 45. Sheikh-Mohamed S, Isho B, Chao GYC, Zuo M, Cohen C, Lustig Y, et al. Systemic
791 and mucosal IgA responses are variably induced in response to SARS-CoV-2
792 mRNA vaccination and are associated with protection against subsequent
793 infection. Mucosal Immunol [Internet]. 2022 May 1 [cited 2023 Nov
794 1];15(5):799. Available from: /pmc/articles/PMC9037584/

795 46. Liew F, Talwar S, Cross A, Willett BJ, Scott S, Logan N, et al. SARS-CoV-2-specific
796 nasal IgA wanes 9 months after hospitalisation with COVID-19 and is not induced
797 by subsequent vaccination. EBioMedicine. 2023 Jan 1;87:104402.

798 47. Fodor E, Devenish L, Engelhardt OG, Palese P, Brownlee GG, García-Sastre A.
799 Rescue of Influenza A Virus from Recombinant DNA. J Virol [Internet]. 1999 Nov
800 [cited 2023 Sep 23];73(11):9679. Available from: /pmc/articles/PMC113010/

801 48. Courtney DG, Chalem A, Bogerd HP, Law BA, Kennedy EM, Holley CL, et al.
802 Extensive epitranscriptomic methylation of A and C residues on murine leukemia
803 virus transcripts enhances viral gene expression. mBio. 2019;10(3):e01209-19.

804 49. Queiroz RML, Smith T, Villanueva E, Marti-Solano M, Monti M, Pizzinga M, et al.
805 Comprehensive identification of RNA–protein interactions in any organism using
806 orthogonal organic phase separation (OOPS). Nature Biotechnology 2019 37:2
807 [Internet]. 2019 Jan 3 [cited 2024 Feb 15];37(2):169–78. Available from:
808 https://www.nature.com/articles/s41587-018-0001-2

809 50. Cox J, Mann M. MaxQuant enables high peptide identification rates,
810 individualized p.p.b.-range mass accuracies and proteome-wide protein

811 quantification. Nature Biotechnology 2008 26:12 [Internet]. 2008 Nov 30 [cited
812 2023 Sep 21];26(12):1367–72. Available from:
813 https://www.nature.com/articles/nbt.1511

814 51. Tyanova S, Temu T, Sinitcyn P, Carlson A, Hein MY, Geiger T, et al. The Perseus
815 computational platform for comprehensive analysis of (prote)omics data.
816 Nature Methods 2016 13:9 [Internet]. 2016 Jun 27 [cited 2023 Sep
817 21];13(9):731–40. Available from:
818 https://www.nature.com/articles/nmeth.3901

819 52. Courtney DG, Tsai K, Bogerd HP, Kennedy EM, Law BA, Emery A, et al.
820 Epitranscriptomic Addition of m5C to HIV-1 Transcripts Regulates Viral Gene
821 Expression. Cell Host Microbe [Internet]. 2019 Aug;26(2):217–27. Available
822 from: https://doi.org/10.1016/j.chom.2019.07.005

823 53. Kawakami E, Watanabe T, Fujii K, Goto H, Watanabe S, Noda T, et al. Strand-
824 specific real-time RT-PCR for distinguishing influenza vRNA, cRNA, and mRNA. J
825 Virol Methods [Internet]. 2011 Apr [cited 2023 Sep 23];173(1):1. Available from:
826 /pmc/articles/PMC3049850/

827 54. Broadbent L, Villenave R, Guo-Parke H, Douglas I, Shields MD, Power UF. In Vitro
828 Modeling of RSV Infection and Cytopathogenesis in Well-Differentiated Human
829 Primary Airway Epithelial Cells (WD-PAECs). Methods Mol Biol [Internet]. 2016
830 [cited 2023 Nov 1];1442:119–39. Available from:
831 https://pubmed.ncbi.nlm.nih.gov/27464691/

832

833

834 **Supplementary data**

835 Supplementary Table 1 – Initial RIC dataset prior to downstream analysis

836 Supplementary Table 2 – RIC dataset of RBP identified in at least 2 replicates of each

837 condition, with fold enrichment and p values included.

838 Supplementary Table 3 – siRNA sequences

839 Supplementary Table 4 – Primer sequences

840 Supplementary Table 5 – Sequences of antisense oligonucleotides

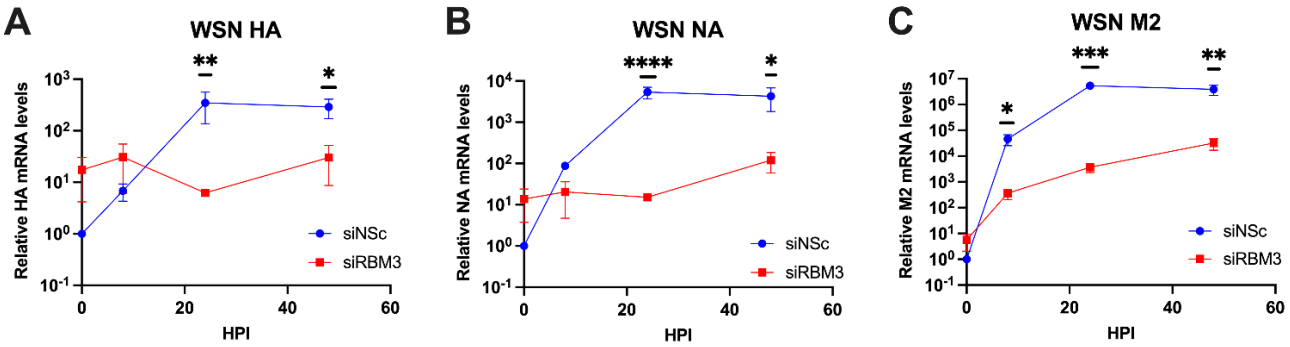

841

842 Supplementary Figure 1 – Growth curve of WSN replication quantified by viral transcript levels

843 Viral transcripts HA (A), NA (B) and M2 (C) were quantified in siRNA transfected A549 cells

844 infected with WSN at MOI 0.01 at 0, 8, 24 and 48 hpi. Cells treated with an RBM3 targeting

845 siRNA (siRBM3) for 48 h prior to infection demonstrated diminished transcript levels

846 compared to a negative control (siNSC) siRNA.